Porous silicon based photoluminescence immunosensor for rapid and highly-sensitive detection of Ochratoxin A

Article *in* Biosensors & Bioelectronics · April 2018

DOI: 10.1016/j.bios.2017.11.048

CITATIONS
23

READS
442

10 authors, including:

Valerii Myndrul
Adam Mickiewicz University
13 PUBLICATIONS **69** CITATIONS

SEE PROFILE

Roman Viter
University of Latvia
111 PUBLICATIONS **1,390** CITATIONS

SEE PROFILE

Donats Erts
University of Latvia
156 PUBLICATIONS **2,416** CITATIONS

SEE PROFILE

Daniels Jevdokimovs
University of Latvia
7 PUBLICATIONS **54** CITATIONS

SEE PROFILE

Biosensors and Bioelectronics 102 (2018) 661–667

Contents lists available at ScienceDirect

Biosensors and Bioelectronics

journal homepage: www.elsevier.com/locate/bios

Porous silicon based photoluminescence immunosensor for rapid and highly-sensitive detection of Ochratoxin A

Valerii Myndrul[a], Roman Viter[b], Maryna Savchuk[c], Nelya Shpyrka[c], Donats Erts[b], Daniels Jevdokimovs[b], Viesturs Silamiķelis[b], Valentyn Smyntyna[a], Arunas Ramanavicius[d], Igor Iatsunskyi[e,*]

[a] Experimental Physics Department, Odessa National I.I. Mechnikov University, 42, Pastera, 65026 Odessa, Ukraine
[b] Institute of Chemical Physics, and Institute of Atomic Physics and Spectroscopy, University of Latvia, 19 Raina Boulevard, LV 1586 Riga, Latvia
[c] National University of Life and Environmental Sciences, 15, Geroyiv Oborony, Kyiv 03041, Ukraine
[d] Department of Physical Chemistry, Institute of Chemistry, Faculty of Chemistry and Geosciences, Vilnius University, Naugarduko 24, LT-03225 Vilnius, Lithuania
[e] NanoBioMedical Centre, Adam Mickiewicz University, 85 Umultowska str., 61-614 Poznan, Poland

ARTICLE INFO

Keywords:
Porous silicon
Ochratoxin A
Photoluminescence
Immobilization of antibodies
Immunosensor

ABSTRACT

A rapid and low cost photoluminescence (PL) immunosensor for the determination of low concentrations of Ochratoxin A (OTA) has been developed. This immunosensor was based on porous silicon (PSi) and modified by antibodies against OTA (anti-OTA). PSi layer was fabricated by metal-assisted chemical etching (MACE) procedure. Main structural parameters (pore size, layer thickness, morphology and nanograins size) and composition of PSi were investigated by means of X-Ray diffraction (XRD), scanning electron microscopy (SEM) and Raman spectroscopy. PL-spectroscopy of PSi was performed at room temperature and showed a wide emission band centered at 680 ± 20 nm. Protein A was covalently immobilized on the surface of PSi, which in next steps was modified by anti-OTA and BSA in this way a anti-OTA/Protein-A/PSi structure sensitive towards OTA was designed. The anti-OTA/Protein-A/PSi-based immunosensors were tested in a wide range of OTA concentrations from 0.001 upto 100 ng/ml. Interaction of OTA with anti-OTA/Protein-A/PSi surface resulted in the quenching of photoluminescence in comparison to bare PSi. The limit of detection (LOD) and the sensitivity range of anti-OTA/Protein-A/PSi immunosensors were estimated. Association constant and Gibbs free energy for the interaction of anti-OTA/Protein-A/PSi with OTA were calculated and analyzed using the interaction isotherms. Response time of the anti-OTA/Protein-A/PSi-based immunosensor toward OTA was in the range of 500–700 s. These findings are very promising for the development of highly sensitive, and potentially portable immunosensors suitable for fast determination of OTA in food and beverages.

1. Introduction

Mycotoxins are toxic secondary metabolites produced by some fungal species. Among all mycotoxins, Ochratoxin A (OTA) has received the most attention due to severe health effects of animals and human (Liang et al., 2015; Malir et al., 2016). OTA is produced by *Aspergillus* and *Penicillium* fungi (O'Callaghan et al., 2003). It has been classified as a possible carcinogen for humans (Heussner and Bingle, 2015). OTA is a mycotoxin, which has been found in foods of plant origin, in human and animal tissues (Afsah-Hejri et al., 2013; Bittner et al., 2013; Jo et al., 2016; Lippolis et al., 2016; Mishra et al., 2016). European Commission (1981/2006 regulation) has recently set maximum tolerated levels (MTL) (R. Liu et al., 2015) of OTA in cereals (5 μg/kg), cocoa (2 μg/kg), beer and grape juice (2 μg/kg) (Covarelli et al., 2012; Quintela et al., 2013). As OTA is present in a number of food products, a development of novel, sensitive and low cost methods for the OTA detection is demanded for control of food quality and protection of human health.

Typically, OTA detection has been performed by various types of chromatography methods (Dohnal et al., 2013; Entwisle et al., 2000; Soleas et al., 2001), or ELISA method (Barna-Vetro et al., 1996). The limit of detection (LOD) of the proposed methods is about 0.15 ng/ml. However, the mentioned methods have some disadvantages. The chromatography methods are time-consuming and expensive. They require experienced and well trained personnel. Despite, ELISA method is simple and reliable. However, the time consuming and the limited sensitivity of ELISA require new alternative technique for OTA detection such as immunosensors.

With intense development of nano- and bio-technologies, a number

* Corresponding author.
E-mail addresses: roman.viter@lu.lv (R. Viter), arunas.ramanavicius@chf.vu.lt (A. Ramanavicius), yatsunskiy@gmail.com (I. Iatsunskyi).

https://doi.org/10.1016/j.bios.2017.11.048
Received 18 August 2017; Received in revised form 13 November 2017; Accepted 15 November 2017
Available online 17 November 2017
0956-5663/

of immunosensors for OTA detection has been developed. Recent approaches of OTA detection by electrochemical (LOD ~ 4.57 pM) (Bougrini et al., 2016), electrical (LOD ~ 0.07 ng/ml) (Mishra et al., 2016), and optical immunosensors (LOD ~ 0.01 nM) (McKeague et al., 2014; C. Wang et al., 2015) have been reported. Aptamer-based biosensing strategy based on an evanescent wave all-fiber (EWA) platform have been developed with LOD values 0.4 nm/ml and 0.3 nM, respectively (L. hua Liu et al., 2015; R. Wang et al., 2015). It was found that the sensitivity to OTA was enhanced through tailoring of bioselective layer, specific to OTA (Bianco et al., 2017; Bueno et al., 2016; Lu et al., 2017). For instance, aptamer based optical sensors showed the highest sensitivity towards OTA in the range of 0.1–10 ng/ml with LOD 0.2 ng/ml (Bianco et al., 2017; Bueno et al., 2016; Lu et al., 2017).

Optical immunosensors are the most perspective among the others (Tereshchenko et al., 2016). Optical technique provides precise detection of optical signal change, induced by adsorption of biomolecules (Viter et al., 2016). Optical immunosensors are portable, compact and compatible with computerized devices and are characterized by low LOD. Therefore, they are suitable for the development Lab-on-Chip-based bioanalytical systems (Viter et al., 2016). Photoluminescence (PL) immunosensors, as a type of optical biosensors, are based on the variation of PL-emission intensity during the interaction of immobilized bio-receptors with target molecules (Jenie et al., 2016; Syshchyk et al., 2015; Viter et al., 2014).

In the recent works we have demonstrated the action of nanostructured PL immunosensors based on specific interaction between antigens and antibodies suitable for the determination of various food pathogens (Viter et al., 2017, 2014, 2012). Such PL immunosensors demonstrated high sensitivity and selectivity towards: antibodies against bovine leukemia viruses (Viter et al., 2012), Salmonella (Viter et al., 2017), OTA (Viter et al., 2018) and aflatoxin (Myndrul et al., 2017).

Porous silicon (PSi) is a well-known template, which is suitable for the development of various biosensors (Dhanekar and Jain, 2013; Roychaudhuri, 2015; Tong et al., 2016; Urmann et al., 2015). Unique physicochemical properties of porous silicon, such as biocompatibility, high surface to volume ratio, tailored surface stoichiometry and simple surface functionalization procedure provide high response of PSi-based biosensors to target analytes. Biosensors based on PSi have been applied for the detection of bacteria (Mathew and Alocilja, 2005), viruses (Rossi et al., 2007) and toxins (Benito-Peña et al., 2016). Stable photoluminescence signal of PSi in visible region is suitable for the development of PL-based biosensors (Dhanekar and Jain, 2013; Jenie et al., 2016; Syshchyk et al., 2015). PSi nanostructures can be fabricated by metal-assisted chemical etching (MACE) (Iatsunskyi et al., 2015a).

In the present study, we report a low cost and sensitive OTA immunosensor based on PSi consequently functionalized with Protein-A, antibodies against OTA (anti-OTA) and then by bovine serum albumin (BSA) (anti-OTA/Protein-A/PSi). Structural and optical properties of the prepared PSi were characterized with scanning electron microscopy (SEM), X-Ray diffraction analysis (XRD) and Raman spectroscopy. Due to high specificity of immobilized anti-OTA towards OTA molecules, the anti-OTA/Protein-A/PSi-based PL-immunosensor showed good sensitivity in a wide range of OTA concentrations 0.01–5 ng/ml with a detection limit of 4.4 pg/ml. According to our best knowledge, this was the first time of the application of anti-OTA/Protein-A/PSi-based PL-immunosensor for the determination of OTA.

2. Materials and methods

2.1. Chemical and reagents

Anti-OTA monoclonal antibodies, OTA, Protein A, bovine serum albumin (BSA) were purchased from Sigma Aldrich.

2.2. The preparation and characterization of PSi

The PSi samples were fabricated from (111) oriented and highly doped p-type Si (B-doped, $\rho = 0.005\ \Omega$ cm) using MACE procedure according to our previous report (Iatsunskyi et al., 2015a). Structural properties of PSi were characterized using grazing incidence X-ray diffraction (GIXRD) by BrukerD5000 from Bruker (Billerica, MA, USA), high resolution field emission scanning electron microscopy (SEM) by SU-70 from Hitachi (Hitachi, Japan) at accelerating voltage of 30 keV and Raman spectroscopy by Renishaw micro-Raman spectrometer equipped with a confocal microscope from Leica (Wetzlar, Germany) and laser ($\lambda_{excitation} = 514$ nm) from Modu-Laser (Centerville, USA).

2.3. The biofunctionalization of the PSi surface

PSi samples were cleaned in Piranha solution (H_2SO_4:H_2O_2 = 4:1), then they were immersed into a 4% solution of APTES in toluene vapors for 1 h at 70 °C. Then samples were removed from the solution and rinsed with toluene and dried at 70 °C for 30 min. The APTES modified PSi samples were washed in PBS and allowed to react with 10% glutaraldehyde in PBS (pH 7.4) for 20 min at room temperature. This was followed by thoroughly rinsing the PSi with DI water to avoid non-specific adsorption of the Protein A. The glutaraldehyde-activated surface was then reacted with 5 μg/ml of Protein A solution in PBS buffer at room temperature for 30 min to form a Protein A layer. Then 5 μg/ml antibodies against Ochratoxin A (anti-OTA) were deposited on PSi samples for covalent capturing by previously immobilized Protein A to provide for the sensing layer the selectivity against OTA (Fig. 1). Finally, 5 μg/ml of BSA was added to block the remaining active sites capable for adsorption of proteins (Fig. 1). As result, anti-OTA/Protein-A/PSi-based structure was formed.

2.4. The evaluation of photoluminescence signal of immunosensor

PL measurements were performed according to the experimental protocol, described in our previous researches (Myndrul et al., 2017; Viter et al., 2018). The PL spectra were excited by UV laser from UltraLasers, Inc. (Toronto, Canada) at output power of 5 mW (λ = 405 nm). The PL spectra were collected by fiber optic spectrometer AvaSpec-ULS3648 from Avantes (Apeldoorn, Netherlands) in the range of 550–900 nm. The PL spectrum was recorded every 15 s within 30 min of the immunosensor interaction with OTA probes. The summarized experimental scheme of PL-immunosensor action is shown in Fig. 2.

3. Results and discussion

3.1. Structural properties of PSi

Fig. 3a shows the plain-view SEM image of macroporous silicon (macro-PSi) obtained by MACE. High-resolution SEM showed that the surface of an individual macropore consists of a mesoporous silicon (meso-PSi) with an average pore size ranged from 10 until 50 nm (Fig. 3b). The average pore size is approximately 2–3 μm, and the thickness of the PSi layer is about 130 μm (Fig. 3c). As it is seen from Fig. 3d, the obtained PSi samples had a rough morphology of the inner surface of the macropore. The microstructure of the obtained PSi structures is affected by isotropic etching and high concentration of holes in silicon (Iatsunskyi et al., 2015c).

XRD spectrum of PSi is shown in Fig. 3e. A strong peak at 2θ = 69,3° was assigned to the (400) plane of crystalline Si. A small peak at around 2θ = 68,9° indicates the presence of PSi layer. The peak position is shifted due to the crystal lattice expansion of PSi (Buttard et al., 1998), which is related to interrelation between the deformation of PSi crystal lattice ($\Delta a/a$) and porosity of PSi (Bellet and Dolino, 1996). We have calculated the deformation $\Delta a/a$ and this value was found as 14 ×

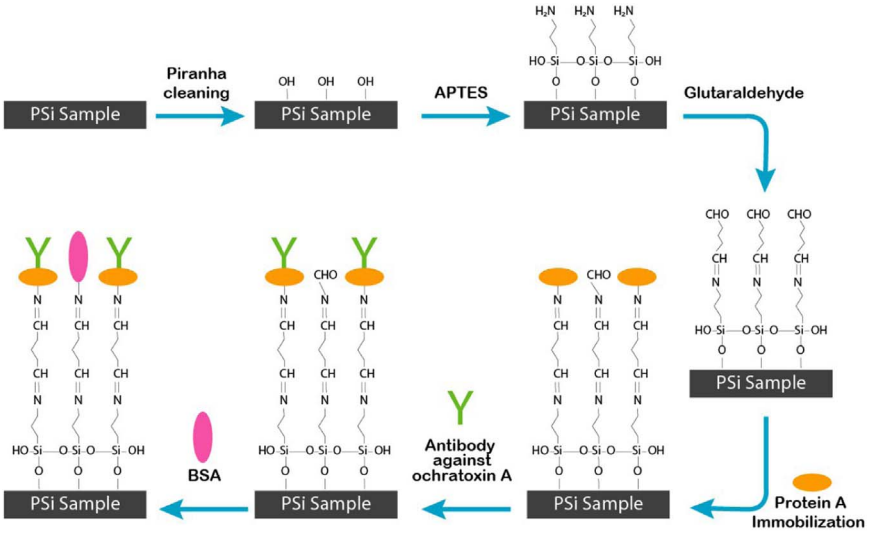

Fig. 1. Functionalization of PSi sample surface by APTES and glutaraldehyde, which is followed by (i) immobilization of Protein A and antibody against OTA and (ii) blockage of surface by BSA.

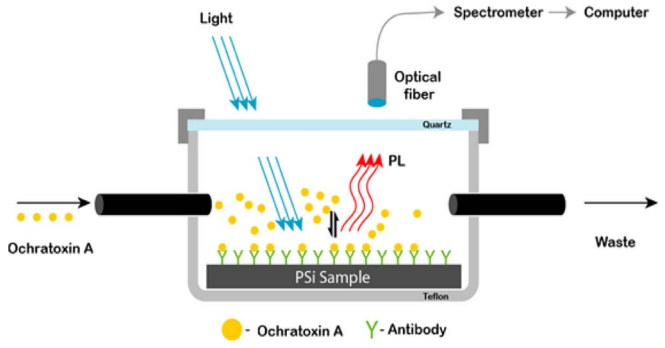

Fig. 2. Experimental setup for OTA detection by PSi-based immunosensor using PL-spectroscopy.

10^{-3}, which corresponds to the porosity of 85%. The mean size of Si nanocrystallites was determined from the full width at half maximum (FWHM) using Scherrer's equation (Iatsunskyi et al., 2015c):

$$D = \frac{0.94\lambda}{FWHM \cdot \cos(\theta)}, \quad (1)$$

where D is the average size of nanocrystallites, λ – the X-ray wavelength (0.154184 nm). The average size of nc-Si was 32 ± 5 nm.

Raman spectra of PSi and Si wafer are presented in Fig. 3e. The main Raman peak (LTO) of PSi was shifted to lower wavenumbers (517 ± 1 cm^{-1}) with consistent increase of its FWHM (11 ± 1 cm^{-1}) comparing to the Si wafer. The Raman shift and the broadening of the LTO peak could be attributed to phonon confinement in quasi-spherical Si nanocrystallites (Iatsunskyi et al., 2015b). This can be used to estimate the average size of nc-Si (Iatsunskyi et al., 2015b). Average value of crystalline size in PSi was calculated using the equation (Iatsunskyi et al., 2015b):

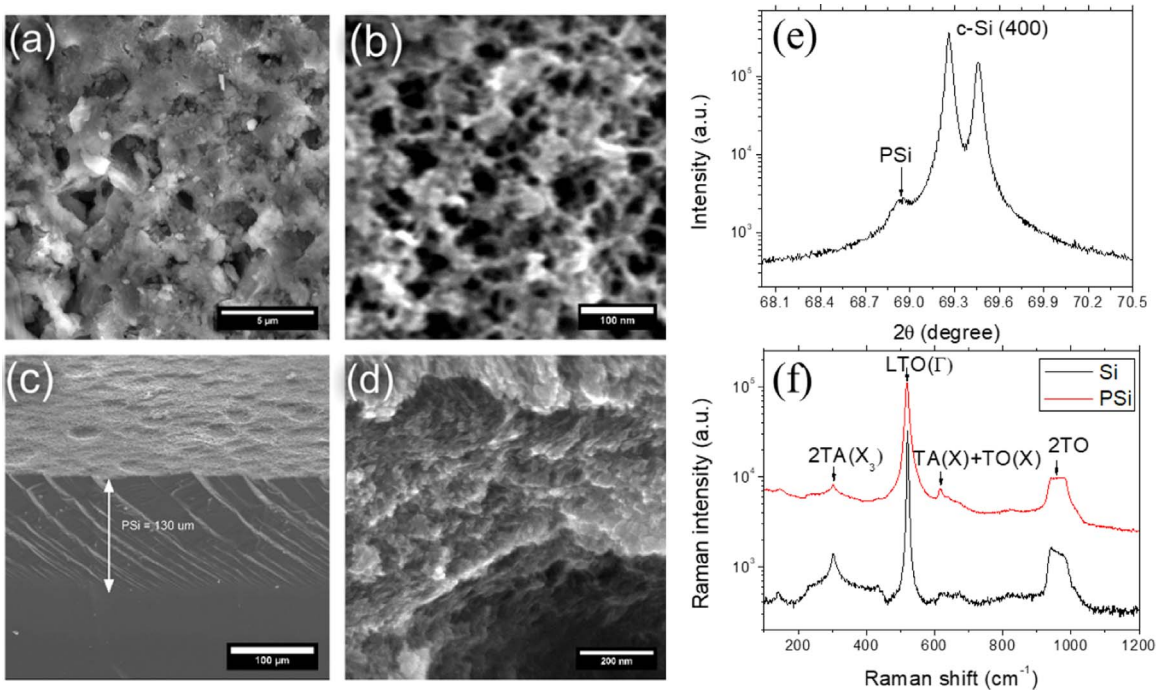

Fig. 3. (a)–(d) SEM images; (e) XRD peak and (f) Raman spectra of PSi (100) sample.

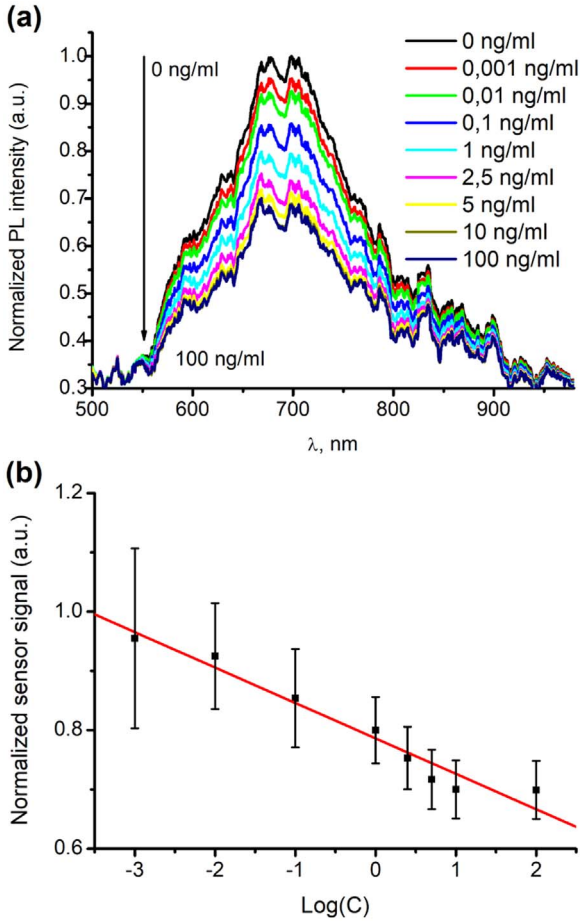

Fig. 4. Photoluminescence spectra of anti-OTA/Protein-A/PSi-based immunosensor after incubation in different OTA concentrations (from top to bottom) containing samples after the reaching of steady state conditions; (b) the dependence of immunosensor signal *vs* OTA concentration, measured at PL peak position (λ = 675 nm).

$$I(\omega) \cong \int_{BZ} \frac{4\pi q^2 \exp\left(-\frac{q^2 L^2}{16\pi^2}\right) d^3q}{(\omega - \omega(q))^2 - \left(\frac{\Gamma_0}{2}\right)^2}; \quad (2)$$

where Γ_0 is the natural line width for Si wafer at room temperature, $\omega = \omega_0 - 120\left(\frac{q}{q_0}\right)^2$, ω_0 is the position of the Si wafer Raman peak. The estimated values of crystalline size in PSi were about 3–4 nm. Properties of obtained structure will be evaluated in correlation with optical properties in the next section.

3.2. The evaluation of PSi photoluminescence during OTA determination

In order to simplify calculations, the PL signal before and after OTA injection was normalized towards PL spectrum of anti-OTA/Protein-A/PSi-based structure before OTA determination. Fig. 4a shows the PL spectrum of PSi with two distinct PL bands, centered at about 675 ± 5 nm (1.84 eV) and 700 ± 5 nm (1.77 eV). The main mechanism of the red emission in PSi is explained by the quantum confinement of electrons from Si nanocrystallites (Bisi et al., 2000). We have calculated the average size of nanocrystallites in the PSi samples using previously reported equation (Myndrul et al., 2017; Salman et al., 2011):

$$E(\text{eV}) = E_g + \frac{h^2}{8d^2}\left[\frac{1}{m_e^*} + \frac{1}{m_h^*}\right], \quad (3)$$

where E(eV) =1.84 / E(eV) = 1.77 eV, E_g = 1.12 eV, h – Planck's constant, $m_e^* = 0.19m_0$; $m_p^* = 0.16m_0$ effective mass electrons and holes in Si, $m_0 = 9.1 \times 10^{-31}$ kg. The calculated average size of nc-Si was about 2.7 ± 1 nm, which corresponds to the values obtained from Raman spectroscopy.

Fig. 4a shows that the PL intensity of anti-OTA/Protein-A/PSi-based structure was quenched by OTA, which specifically bounded to the immobilized anti-OTA. The saturation of analytical signal occurs in OTA concentration range of 5–10 ng/ml (Fig. 4a). Fig. 4b shows the PL intensity of anti-OTA/Protein-A/PSi-based structure at 675 nm, which is plotted in logarithmic scale of OTA concentration. The PL intensity of the immunosensor versus the OTA concentration can be interpolated by the following equation:

$$I_{675} = 0.77 - 0.06 \cdot \lg(C), \quad (4)$$

where C is OTA concentration.

The limit of detection (LOD) was determined using formula (Liu et al., 2016; Myndrul et al., 2017):

$$LOD = 3.3 \cdot \sigma / b, \quad (5)$$

where σ is the standard deviation of negative control and b is the slope of the curve. The calculated value of LOD was approximately 4.4 pg/ml. This calculated value of LOD is almost the same as it was previously obtained for high-sensitive aptamer-based SPR-polarization platform (Zhu et al., 2015).

3.3. Analysis of adsorption isotherms

Adsorption isotherms are providing some information on mechanisms of interaction between the immunosensor surface and target molecules (Viter et al., 2018). Fig. 5a shows a representative time-resolved changes of PL intensity of anti-OTA/Protein-A/PSi-based immunosensor *vs* several OTA concentrations. The sensor response S was calculated according to formula:

$$S(C) = 1 - I_{eq}(C), \quad (6)$$

where I_{eq} and C are the normalized PL signal value of anti-OTA/Protein-A/PSi-based structure in steady state conditions and OTA concentration, respectively.

The adsorption isotherm of OTA interaction with anti-OTA/Protein-A/PSi-based immunosensor is shown in Fig. 5b.

Calculations reveals that the interaction of the analyte (OTA) occurred according to the first order kinetics (Ratautaite et al., 2015):

$$\frac{dN}{dt} = k_a \cdot C \cdot (N_s - N) - k_d \cdot N. \quad (7)$$

At steady state conditions when the $\frac{dN}{dt} = 0$, the isotherm of analyte (OTA) interaction was analyzed using Langmuir (8) and Langmuir-Freundlich (9) equations (Myndrul et al., 2017; Viter et al., 2018):

$$\theta = \frac{B \cdot C}{K_D + C}, \quad (8)$$

$$\theta = \frac{B \cdot C^n}{K_D^n + C^n}, \quad (9)$$

where $\theta = \frac{N}{N_s}$ is surface coverage, $K_D = \frac{k_d}{k_a}$ is affinity constant and n is power coefficient.

Power coefficient 'n', which was calculated using Eqs. (8) and (9), is lower than 1 (n < 1). Therefore, such value of power coefficient is pointing the significant interaction between OTA, which is present in solution, and anti-OTA, which is present on the interphase of anti-OTA/Protein-A/PSi-based immunosensor. The analysis of the adsorption isotherms showed better fitting using Langmuir-Freundlich equation (Fig. 5b). The obtained values of n and K_D are shown in the Table 1. It points to the limitation of protein adsorption by high surface area of the anti-OTA/Protein-A/PSi-based immunosensor and additional diffusion process of the OTA molecules within the pores of modified PSi.

The interaction between OTA, which is present in the sample, and anti-OTA, which is present in anti-OTA/Protein-A/PSi-based

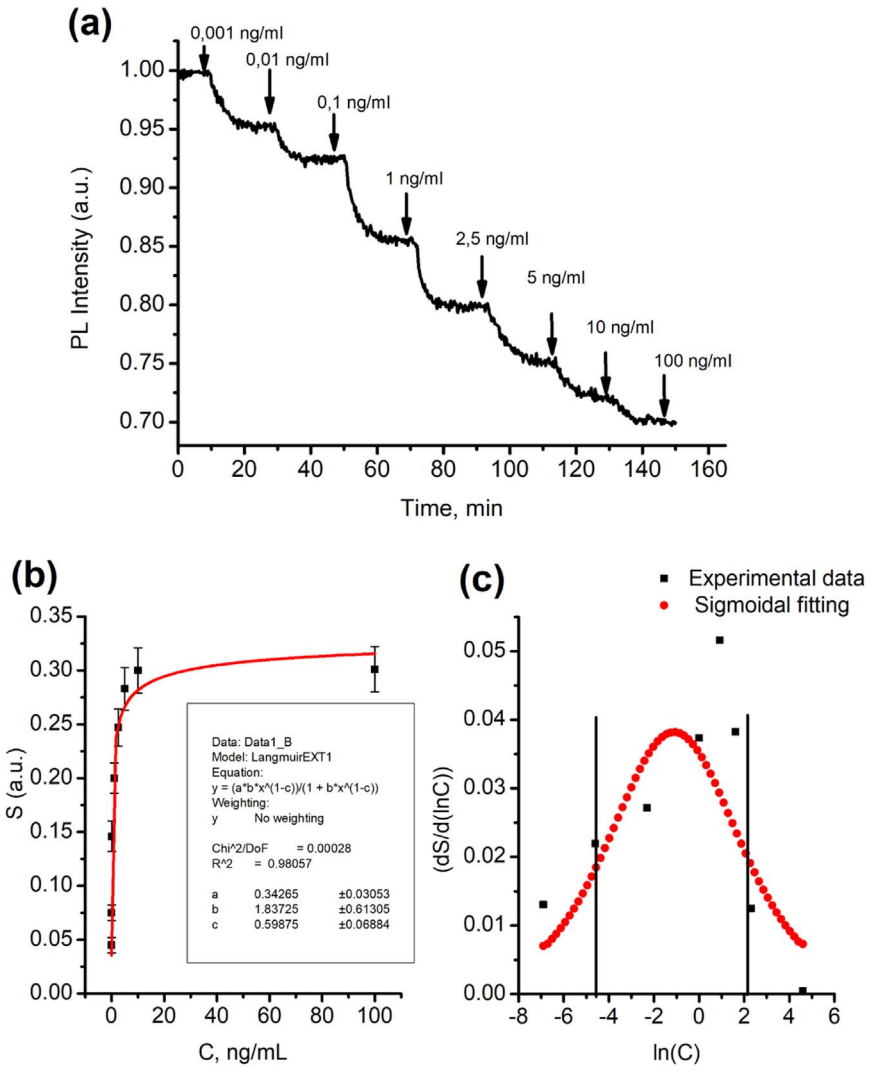

Fig. 5. Dependence of PL peak maximum (at λ = 675 nm) *vs* OTA concentration; (b) the isotherm of analyte (OTA) interaction with anti-OTA/Protein-A/PSi-based immunosensor; and (c) calculated sensitivity of anti-OTA/Protein-A/PSi-based immunosensor towards OTA.

Table 1
Calculated parameters of OTA adsorption.

n	K_D, ng/ml	K_D, M	ΔG, kJ/mol
0.4 ± 0.02	0.22 ± 0.03	$5.4{\cdot}10^{-10} \pm 0.3{\cdot}10^{-11}$	−53.1 ± 2.7

immunosensor can be estimated by the calculation of Gibbs free energy (Δ*G*) according to equation:

$$\Delta G = -R{\cdot}T{\cdot}\ln(K_{D0}), \tag{10}$$

where *T* and *R* are absolute temperature and universal gas constant, respectively. The value of K_{D0} was calculated as:

$$K_{D0} = \frac{K_D}{C}, \tag{11}$$

where *C* is the OTA concentration, which in this calculation was equal to 1 M.

Decrease of the Gibbs free energy point to a strength of interaction between the surface and the target biomolecule. It was reported, that Δ*G* value for OTA molecules varies in the range of −28 to −38 kJ/mol (Barna-Vetro et al., 1996; Soleas et al., 2001). The present calculations points to even stronger interaction (Δ*G* = −53.1 kJ/mol) between OTA and anti-OTA/Protein-A/PSi-based immunosensor surface. The obtained Δ*G* values correlate with the ones reported in (Myndrul et al., 2017; Viter et al., 2018). We suppose that the increase of Δ*G* value might be related to better orientation of anti-OTA due to applied Protein A based layer, which was deposited on the PSi surface and is specifically binding antibodies via Fc-region, which is in the 'tail' of antibody. Therefore in such way immobilized anti-OTA antibodies become uniformly and properly oriented on the surface of designed immunosensor's (Makaraviciute et al., 2015).

Sensitivity of the immunosensors was calculated as a derivative of the sensor signal *S* to the natural logarithm of OTA concentration *C* (Fig. 5c) (Myndrul et al., 2017; Viter et al., 2018). In addition, a differentiated data plot of fitted Sigmoid function was built for the comparison with experimental data. Analysis of the sensitivity showed, that anti-OTA/Protein-A/PSi-based immunosensor showed the sensitivity towards OTA in the range of 0.01–5 ng/ml (Fig. 5c). This shows sensitivity towards OTA, even better than the ELISA method, reported previously (Jodra et al., 2015; Viter et al., 2018; Yang et al., 2015).

The PL quenching of anti-OTA/Protein-A/PSi-based immunosensor, was induced by OTA interaction with immobilized anti-OTA. The PL quenching mechanisms can rely on several factors: (i) energy transfer between PSi and anti-OTA/Protein-A/PSi-based structure, which is interacting with OTA, (ii) charge transfer, (iii) Fermi level shift during OTA interaction with Protein-A/anti-OTA&BSA-based structure, (iv) and change of dielectric constant of the surrounding media during increase of OTA concentrations (Chvojka et al., 2004; Dhanekar et al., 2010; Harper and Sailor, 1997; Syshchyk et al., 2015). However, we have no facilities to measure additional parameters of the

immunosensor (conductivity, work function, etc.) simultaneously with PL measurements. But based on previously reported results and general knowledge about in this experiment used proteins we can exclude energy and charge transfer between PSi and anti-OTA/Protein-A/PSi-based structure as a possible mechanisms of PL quenching (Tereshchenko et al., 2016; Viter et al., 2018, 2017). We suppose that Fermi level shift during analyte adsorption and change of dielectric constant of the media, which is in close proximity to PL-sites of PSi, is the most plausible mechanisms of PL quenching in here reported system. Hence, the PL is quenched due to changes of local electric field near PSi surface through the interaction of OTA molecules with anti-OTA, which is present in the anti-OTA/Protein-A/PSi-based structure. Actually, understanding of the mechanisms of PL quenching still requires more experiments and analysis. It will be a topic for next research paper.

4. Conclusions

The investigation of optical properties of PSi showed that it is very promising material for the development of PL-based immunosensors. PL spectroscopy based immunosensor for the determination of OTA was developed using step-by-step modification of PSi surface with Protein A, anti-OTA and BSA. Developed anti-OTA/Protein-A/PSi/ structure showed good sensitivity towards OTA. The anti-OTA /Protein-A/PSi-based immunosensor was integrated within portable fiber optics based measurement system. In this research reported design of immunosensor is suitable for direct and real time detection of toxins and other analytes, which could be used in the monitoring of food quality. It was shown that the decrease of the PL-intensity of anti-OTA /Protein-A/PSi-based structure is observed with the increase of OTA concentration in the samples used for investigations. Therefore, this decrease of PL was interpreted as analytical signal. The response time of the immunosensor to different OTA concentrations was in the range of 500–700 s. The developed immunosensor showed good sensitivity towards OTA in concentration range of 0.01–5 ng/ml with detection limit of 4.4 pg/ml. Langmuir-Freundlich isotherms were plotted for the interaction of OTA with anti-OTA /Protein-A/PSi-based structure, and some aspects of interaction mechanisms and PL quenching mechanisms are discussed. Further investigations will be focused on the evaluation of immunosensor performance and better understanding of interactions between analytes and biological recognition and signal transduction parts used in immunosensor design.

Acknowledgment

I.I. acknowledges the financial support from the National Science Centre of Poland by the SONATA 11 project UMO-2016/21/D/ST3/00962. R.V acknowledges the financial support from BIOSENSORSAGRICULT (Development of nanotechnology based biosensors for agriculture FP7-PEOPLE-2012-IRSES, contract nr. 318520). A.R. acknowledges the financial support from Lithuanian Research Council (TAP LZ-3/2015). The authors are thankful to prof. N. Starodub for support with biological samples.

References

Afsah-Hejri, L., Jinap, S., Hajeb, P., Radu, S., Shakibazadeh, S., 2013. A review on mycotoxins in food and feed: Malaysia case study. Compr. Rev. Food Sci. Food Saf. 12, 629–651. http://dx.doi.org/10.1111/1541-4337.12029.

Barna-Vetro, I., Solti, L., Teren, J., Gyongyosi, A., Szabo, E., Wolfling, A., 1996. Sensitive ELISA test for determination of ochratoxin A. J. Agric. Food Chem. 44, 4071–4074.

Bellet, D., Dolino, G., 1996. X-ray diffraction studies of porous silicon. Thin Solid Films 276, 1–6.

Benito-Peña, E., Valdés, M.G., Glahn-Martínez, B., Moreno-Bondi, M.C., 2016. Fluorescence based fiber optic and planar waveguide biosensors. A review. Anal. Chim. Acta 943, 17–40. http://dx.doi.org/10.1016/j.aca.2016.08.049.

Bianco, M., Sonato, A., De Girolamo, A., Pascale, M., Romanato, F., Rinaldi, R., Arima, V., 2017. An aptamer-based SPR-polarization platform for high sensitive OTA detection. Sens. Actuators B Chem. 241, 314–320. http://dx.doi.org/10.1016/j.snb.2016.10.056.

Bisi, O., Ossicini, S., Pavesi, L., Bisi, O., Ossicini, S., Pavesi, L., 2000. Porous silicon: a quantum sponge structure for silicon based optoelectronics. Surf. Sci. Rep. 38, 1–126. http://dx.doi.org/10.1016/S0167-5729(99)00012-6.

Bittner, A., Cramer, B., Humpf, H.-U., 2013. Matrix binding of ochratoxin A during roasting. J. Agric. Food Chem. 61, 12737–12743. http://dx.doi.org/10.1021/jf403984x.

Bougrini, M., Baraket, A., Jamshaid, T., Aissari, A., El, Bausells, J., Zabala, M., Bari, N., El, Bouchikhi, B., Jaffrezic-Renault, N., Abdelhamid, E., Zine, N., 2016. Development of a novel capacitance electrochemical biosensor based on silicon nitride for ochratoxin A detection. Sens. Actuators B: Chem. http://dx.doi.org/10.1016/j.snb.2016.03.166.

Bueno, D., Muñoz, R., Marty, J.L., 2016. Fluorescence analyzer based on smartphone camera and wireless for detection of ochratoxin A. Sens. Actuators B Chem. 232, 462–468. http://dx.doi.org/10.1016/j.snb.2016.03.140.

Buttard, D., Dolino, G., Bellet, D., Baumbach, T., Rieutord, F., 1998. X-ray reflectivity investigation of thin p-type porous silicon layers. Solid State Commun. 109, 1–5. http://dx.doi.org/10.1016/S0038-1098(98)00531-6.

Chvojka, T., Vrkoslav, V., Jelínek, I., Jindřich, J., Lorenc, M., Dian, J., 2004. Mechanisms of photoluminescence sensor response of porous silicon for organic species in gas and liquid phases. Sens. Actuators B Chem. 100, 246–249. http://dx.doi.org/10.1016/j.snb.2003.12.040.

Covarelli, L., Beccari, G., Marini, A., Tosi, L., 2012. A review on the occurrence and control of ochratoxigenic fungal species and ochratoxin A in dehydrated grapes, non-fortified dessert wines and dried vine fruit in the Mediterranean area. Food Control. http://dx.doi.org/10.1016/j.foodcont.2012.01.044.

Dhanekar, S., Jain, S., 2013. Porous silicon biosensor: current status. Biosens. Bioelectron. http://dx.doi.org/10.1016/j.bios.2012.09.045.

Dhanekar, S., Islam, S.S., Islam, T., Harsh, 2010. Highly sensitive porous silicon sensor: detection of organic vapours using photoluminescence quenching technique. Int. J. Smart Sens. Intell. Syst. 3, 1–13.

Dohnal, V., Dvořák, V., Malíř, F., Ostrý, V., Roubal, T., 2013. A comparison of ELISA and HPLC methods for determination of ochratoxin A in human blood serum in the Czech Republic. Food Chem. Toxicol. 62, 427–431. http://dx.doi.org/10.1016/j.fct.2013.09.010.

Entwisle, A.C., Williams, A.C., Mann, P.J., Slack, P.T., Gilbert, J., Burdaspal, P., Eklund, E., Gardikis, J., Hald, B., Herry, M.P., Jørgensen, K., Kandler, H., Maas, R., Martins, M.L., Patel, S., Schuster, M., Solfrizzo, M., Strassmeir, E., Tiebach, R., Trogersen, T., 2000. Liquid chromatographic method with immunoaffinity column cleanup for determination of ochratoxin A in barley: collaborative study. J. AOAC Int. 83, 1377–1386.

Harper, J., Sailor, M.J., 1997. Photoluminescence quenching and the photochemical oxidation of porous silicon by molecular oxygen. Langmuir 13, 4652–4658. http://dx.doi.org/10.1021/la960535z.

Heussner, A.H., Bingle, L.E.H., 2015. Comparative ochratoxin toxicity: a review of the available data. Toxins (Basel). http://dx.doi.org/10.3390/toxins7104253.

Iatsunskyi, I., Jancelewicz, M., Nowaczyk, G., Kempiński, M., Peplińska, B., Jarek, M., Załęski, K., Jurga, S., Smyntyna, V., 2015a. Atomic layer deposition TiO2 coated porous silicon surface: structural characterization and morphological features. Thin Solid Films 589, 303–308. http://dx.doi.org/10.1016/j.tsf.2015.05.056.

Iatsunskyi, I., Nowaczyk, G., Jurga, S., Fedorenko, V., Pavlenko, M., Smyntyna, V., 2015b. One and two-phonon Raman scattering from nanostructured silicon. Opt. – Int. J. Light Electron Opt. 126, 1650–1655. http://dx.doi.org/10.1016/j.ijleo.2015.05.088.

Iatsunskyi, I., Pavlenko, M., Viter, R., Jancelewicz, M., Nowaczyk, G., Baleviciute, I., Załęski, K., Jurga, S., Ramanavicius, A., Smyntyna, V., 2015c. Tailoring the structural, optical, and photoluminescence properties of porous silicon/TiO 2 nanostructures. J. Phys. Chem. C 119, 7164–7171. http://dx.doi.org/10.1021/acs.jpcc.5b01670.

Jenie, S.N.A., Plush, S.E., Voelcker, N.H., 2016. Recent advances on luminescent enhancement-based porous silicon biosensors. Pharm. Res. 33, 2314–2336. http://dx.doi.org/10.1007/s11095-016-1889-1.

Jo, E.J., Mun, H., Kim, S.J., Shim, W.B., Kim, M.G., 2016. Detection of ochratoxin A (OTA) in coffee using chemiluminescence resonance energy transfer (CRET) aptasensor. Food Chem. 194, 1102–1107. http://dx.doi.org/10.1016/j.foodchem.2015.07.152.

Jodra, A., Hervás, M., López, M.Á., Escarpa, A., 2015. Disposable electrochemical magneto immunosensor for simultaneous simplified calibration and determination of ochratoxin A in coffee samples. Sens. Actuators B Chem. 221, 777–783. http://dx.doi.org/10.1016/j.snb.2015.07.007.

Liang, R., Shen, X.L., Zhang, B., Li, Y., Xu, W., Zhao, C., Luo, Y., Huang, K., 2015. Apoptosis signal-regulating kinase 1 promotes ochratoxin A-induced renal cytotoxicity. Sci. Rep. 5, 8078. http://dx.doi.org/10.1038/srep08078.

Lippolis, V., Ferrara, M., Cervellieri, S., Damascelli, A., Epifani, F., Pascale, M., Perrone, G., 2016. Rapid prediction of ochratoxin A-producing strains of Penicillium on dry-cured meat by MOS-based electronic nose. Int. J. Food Microbiol. 218, 71–77. http://dx.doi.org/10.1016/j.ijfoodmicro.2015.11.011.

Liu, L. hua, Zhou, X. hong, Shi, H. chang, 2015. Portable optical aptasensor for rapid detection of mycotoxin with a reversible ligand-grafted biosensing surface. Biosens. Bioelectron. 72, 300–305. http://dx.doi.org/10.1016/j.bios.2015.05.033.

Liu, R., Huang, Y., Ma, Y., Jia, S., Gao, M., Li, J., Zhang, H., Xu, D., Wu, M., Chen, Y., Zhu, Z., Yang, C., 2015. Design and synthesis of target-responsive aptamer-cross-linked hydrogel for visual quantitative detection of ochratoxin A. ACS Appl. Mater. Interfaces 7, 6982–6990. http://dx.doi.org/10.1021/acsami.5b01120.

Liu, Y., Yu, J., Wang, Y., Liu, Z., Lu, Z., 2016. An ultrasensitive aptasensor for detection of ochratoxin A based on shielding effect-induced inhibition of fluorescence resonance energy transfer. Sens. Actuators B Chem. 222, 797–803. http://dx.doi.org/10.1016/j.

snb.2015.09.007.
Lu, Z., Chen, X., Hu, W., 2017. A fluorescence aptasensor based on semiconductor quantum dots and MoS2 nanosheets for ochratoxin A detection. Sens. Actuators B Chem. 246, 61–67. http://dx.doi.org/10.1016/j.snb.2017.02.062.
Makaraviciute, A., Ramanavicius, A., Ramanaviciene, A., 2015. Development of areusable protein G based SPR immunosensor for direct human growth hormonedetection in real samples. Anal. Methods 7 (23), 9875–9884.
Malir, F., Ostry, V., Pfohl-Leszkowicz, A., Malir, J., Toman, J., 2016. Ochratoxin A: 50 years of research. Toxins (Basel). http://dx.doi.org/10.3390/toxins8070191.
Mathew, F.P., Alocilja, E.C., 2005. Porous silicon-based biosensor for pathogen detection. Biosens. Bioelectron. 20, 1656–1661. http://dx.doi.org/10.1016/j.bios.2004.08.006.
McKeague, M., Velu, R., Hill, K., Bardóczy, V., Mészáros, T., DeRosa, M., 2014. Selection and characterization of a novel DNA aptamer for label-free fluorescence biosensing of ochratoxin A. Toxins (Basel) 6, 2435–2452. http://dx.doi.org/10.3390/toxins6082435.
Mishra, R.K., Hayat, A., Catanante, G., Istamboulie, G., Marty, J.L., 2016. Sensitive quantitation of ochratoxin A in cocoa beans using differential pulse voltammetry based aptasensor. Food Chem. 192, 799–804. http://dx.doi.org/10.1016/j.foodchem.2015.07.080.
Myndrul, V., Viter, R., Savchuk, M., Koval, M., Starodub, N., Silamiķelis, V., Smyntyna, V., Ramanavicius, A., Iatsunskyi, I., 2017. Gold coated porous silicon nanocomposite as a substrate for photoluminescence-based immunosensor suitable for the determination of aflatoxin B1. Talanta. http://dx.doi.org/10.1016/j.talanta.2017.07.054.
O'Callaghan, J., Caddick, M.X., Dobson, A.D.W., 2003. A polyketide synthase gene required for ochratoxin A biosynthesis in Aspergillus ochraceus. Microbiology 149, 3485–3491. http://dx.doi.org/10.1099/mic.0.26619-0.
Quintela, S., Villarán, M.C., López de Armentia, I., Elejalde, E., 2013. Ochratoxin A removal in wine: a review. Food Control 30, 439–445. http://dx.doi.org/10.1016/j.foodcont.2012.08.014.
Ratautaite, V., Plausinaitis, D., Baleviciute, I., Mikoliunaite, L., Ramanaviciene, A., Ramanavicius, A., 2015. Characterization of caffeine-imprinted polypyrrole by a quartz crystal microbalance and electrochemical impedance spectroscopy. Sens. Actuators B Chem. 212, 63–71. http://dx.doi.org/10.1016/j.snb.2015.01.109.
Rossi, A.M., Wang, L., Reipa, V., Murphy, T.E., 2007. Porous silicon biosensor for detection of viruses. Biosens. Bioelectron. 23, 741–745. http://dx.doi.org/10.1016/j.bios.2007.06.004.
Roychaudhuri, C., 2015. A review on porous silicon based electrochemical biosensors: beyond surface area enhancement factor. Sens. Actuators B Chem. 210, 310–323. http://dx.doi.org/10.1016/j.snb.2014.12.089.
Salman, K.A., Omar, K., Hassan, Z., 2011. The effect of etching time of porous silicon on solar cell performance. Superlattices Microstruct. 50, 647–658. http://dx.doi.org/10.1016/j.spmi.2011.09.006.
Soleas, G.J., Yan, J., Goldberg, D.M., 2001. Assay of ochratoxin A in wine and beer by high-pressure liquid chromatography photodiode array and gas chromatography mass selective detection. J. Agric. Food Chem. 49, 2733–2740. http://dx.doi.org/10.1021/jf0100651.
Syshchyk, O., Skryshevsky, V.A., Soldatkin, O.O., Soldatkin, A.P., 2015. Enzyme biosensor systems based on porous silicon photoluminescence for detection of glucose, urea and heavy metals. Biosens. Bioelectron. 66, 89–94.
Tereshchenko, A., Bechelany, M., Viter, R., Khranovskyy, V., Smyntyna, V., Starodub, N., Yakimova, R., 2016. Optical biosensors based on ZnO nanostructures: advantages and perspectives. A review. Sens. Actuators B Chem. http://dx.doi.org/10.1016/j.snb.2016.01.099.
Tong, W.Y., Sweetman, M.J., Marzouk, E.R., Fraser, C., Kuchel, T., Voelcker, N.H., 2016. Towards a subcutaneous optical biosensor based on thermally hydrocarbonised porous silicon. Biomaterials 74, 217–230. http://dx.doi.org/10.1016/j.biomaterials.2015.09.045.
Urmann, K., Walter, J.-G., Scheper, T., Segal, E., 2015. Label-free optical biosensors based on aptamer-functionalized porous silicon scaffolds. Anal. Chem. 87, 1999–2006. http://dx.doi.org/10.1021/ac504487g.
Viter, R., Smyntyna, V., Starodub, N., Tereshchenko, A., Kusevitch, A., Doychoa, I., Geveluk, S., Slishik, N., Buk, J., Duchoslav, J., Lubchuk, J., Konup, I., Ubelis, A., Spigulis, J., 2012. Novel immune TiO2 photoluminescence biosensors for leucosis detection. Procedia Eng. 47, 338–341. http://dx.doi.org/10.1016/j.proeng.2012.09.152.
Viter, R., Khranovskyy, V., Starodub, N., Ogorodniichuk, Y., Gevelyuk, S., Gertnere, Z., Poletaev, N., Yakimova, R., Erts, D., Smyntyna, V., Ubelis, A., 2014. Application of room temperature photoluminescence from ZnO nanorods for Salmonella detection. IEEE Sens. J. 14, 2028–2034. http://dx.doi.org/10.1109/JSEN.2014.2309277.
Viter, R., Jekabsons, K., Kalnina, Z., Poletaev, N., Hsu, S.H., Riekstina, U., 2016. Bioanalytical system for detection of cancer cells with photoluminescent ZnO nanorods. Nanotechnology 27, 465101. http://dx.doi.org/10.1088/0957-4484/27/46/465101.
Viter, R., Tereshchenko, A., Smyntyna, V., Ogorodniichuk, J., Starodub, N., Yakimova, R., Khranovskyy, V., Ramanavicius, A., 2017. Toward development of optical biosensors based on photoluminescence of TiO2 nanoparticles for the detection of Salmonella. Sens. Actuators B Chem. 252, 95–102. http://dx.doi.org/10.1016/j.snb.2017.05.139.
Viter, R., Savchuk, M., Iatsunskyi, I., Pietralik, Z., Starodub, N., Shpyrka, N., Ramanaviciene, A., Ramanavicius, A., 2018. Analytical, thermodynamical and kinetic characteristics of photoluminescence immunosensor for the determination of ochratoxin A. Biosens. Bioelectron. 99, 237–243. http://dx.doi.org/10.1016/j.bios.2017.07.056.
Wang, C., Dong, X., Liu, Q., Wang, K., 2015. Label-free colorimetric aptasensor for sensitive detection of ochratoxin A utilizing hybridization chain reaction. Anal. Chim. Acta 860, 83–88. http://dx.doi.org/10.1016/j.aca.2014.12.031.
Wang, R., Xiang, Y., Zhou, X., Liu, L. hua, Shi, H., 2015. A reusable aptamer-based evanescent wave all-fiber biosensor for highly sensitive detection of ochratoxin A. Biosens. Bioelectron. 66, 11–18. http://dx.doi.org/10.1016/j.bios.2014.10.079.
Yang, J., Gao, P., Liu, Y., Li, R., Ma, H., Du, B., Wei, Q., 2015. Label-free photoelectrochemical immunosensor for sensitive detection of ochratoxin A. Biosens. Bioelectron. 64, 13–18. http://dx.doi.org/10.1016/j.bios.2014.08.025.
Zhu, Z., Feng, M., Zuo, L., Zhu, Z., Wang, F., Chen, L., Li, J., Shan, G., Luo, S.-Z., 2015. An aptamer based surface plasmon resonance biosensor for the detection of ochratoxin A in wine and peanut oil. Biosens. Bioelectron. 65, 320–326. http://dx.doi.org/10.1016/j.bios.2014.10.059.